Heterotrimeric G protein signaling governs the cortical stability during apical constriction in *Drosophila* gastrulation

Takuma Kanesaki[a,b,c], Susumu Hirose[a,b], Joerg Grosshans[c], and Naoyuki Fuse[a,b,d,*]

[a] Department of Developmental Genetics, National Institute of Genetics, 1111 Yata, Mishima, 411-8540 Shizuoka, Japan

[b] Division of Genetics, SOKENDAI, 1111 Yata, Mishima, Shizuoka-ken, 411-8540, Japan.

[c] Institut für Biochemie und Molekulare Zellbiologie, Georg-Augst-Universitaet Goettingen, Justus-von-Liebig-Weg 11, 37077 Göttingen, Germany

d Laboratory for Molecular Developmental Biology, Graduate School of Science, Kyoto University, Kitashirakawa-Oiwake, Sakyo-ku, Kyoto 606-8502, Japan

* Corresponding Author, Tel: +81-75-753-4261, e-mail: nfuse@gcoe.biol.sci.kyoto-u.ac.jp

Abstract

During gastrulation in *Drosophila melanogaster,* coordinated apical constriction of the cellular surface drives invagination of the mesoderm anlage. Forces generated by the cortical cytoskeletal network have a pivotal role in this cellular shape change. Here, we show that the organisation of cortical actin is essential for stabilisation of the cellular surface against contraction. We found that mutation of genes related to heterotrimeric G protein (HGP) signaling, such as *Gβ13F*, *Gγ1*, and *ric-8*, results in formation of blebs on the ventral cellular surface. The formation of blebs is caused by perturbation of cortical actin and induced by local surface contraction. HGP signaling mediated by two Gα subunits, Concertina and G-iα65A, constitutively regulates actin organisation. We propose that the organisation of cortical actin by HGP is required to reinforce the cortex so that the cells can endure hydrostatic stress during tissue folding.

Highlights: > In *Drosophila* mesoderm invagination, Fog signaling induces apical constriction of ventral cells. > We found that heterotrimetic G protein and its regulator Ric-8 are required not only for Fog signaling but also for the organisation of cortical actin. > Partial disruption of cortical actin induced membrane blebbing during apical constriction. > The heterotrimeric G protein pathway confers physical stability on the cellular surface during morphogenesis.

Key words: *Drosophila*; Gastrulation; Cortical actin; Heterotrimeric G protein; Bleb

1. Introduction

The coordinated movement of cells is one of the foundations of tissue morphogenesis. The forces driving the cellular movements are generated by surface dynamics, such as rearrangements of cell adhesions and changes of the contractility of cortical acto-myosin networks (reviewed in Lecuit and Lenne, 2007). However, the surface mechanics resisting deformation forces and maintaining cortical integrity are not well understood.

The shape of the cell surface can change dynamically. One notable surface feature is the bleb, a spherical protrusion of the plasma membrane observed in diverse cellular processes such as locomotion, division, and apoptosis. Formation of blebs is driven by hydrostatic pressure in the cytoplasm. According to the current model, blebbing starts with local compression of the cytoskeletal network and proceeds according to a subsequent increase of the pressure (Charras et al., 2005). The compression of the cytoskeleton is mediated by the contractile force of non-muscle myosin II (MyoII). Though it has been shown that various cells, such as germ line and cancer cells, utilise blebs for their motility (Blaser et al., 2006; Kardash et al., 2010; reviewed in Fackler and Grosse, 2008), the role of blebs and the mechanism of blebbing in tissue morphogenesis are still largely unclear.

Invagination of a cellular layer is one of the common events in tissue morphogenesis. In gastrulation in *Drosophila*, ventral cells of the blastoderm embryo invaginate and then differentiate to mesoderm (Sweeton et al., 1991; Costa et al., 1993). The process of mesoderm invagination can be grossly divided

into two sequential steps: apical constriction and furrow internalisation. During apical constriction, ventral cells collectively contract their apices and consequently form a shallow furrow on the embryo. During furrow internalisation, the ventral furrow becomes deeper and the layer of cells becomes engulfed in the embryonic body (Fig. 1A and B). The molecular and cellular mechanisms underlying apical constriction have been studied extensively. The change of cellular shape is mediated by integrated functioning of the cortical acto-myosin network and cellular adherens junction complex (Dawes-Hoang et al., 2005; Fox and Peifer, 2007; Martin et al., 2009). The force driving the constriction is generated by pulsed contractility of MyoII (Martin et al., 2009). The tensile force from individual cells is transmitted to epithelial tissue through the adherens junction, and the tissue generates feedback force that leads to anisotropic constriction of ventral cells (Martin et al., 2010).

Heterotrimeric G protein (HGP) has an important role in apical constriction in *Drosophila* gastrulation. Signaling triggered by the extracellular ligand *folded gastrulation* (*fog*) promotes surface accumulation of MyoII in ventral cells, and the Fog signaling is mediated through an HGP α subunit encoded by *concertina* (*cta*) (Parks and Wieschaus, 1991; Costa et al., 1994; Morize et al., 1998; Dawes-Hoang et al., 2005). HGP belongs to the GTPase family, and its activity is regulated by multiple factors, including guanine nucleotide exchange factor (GEF). A previous study showed that *ric-8* mutation results in a twisted germ-band due to abnormal mesoderm invagination (Hampoelz et al., 2005). *ric-8* was first identified as a gene responsible for synaptic transmission in *Caenorhabditis*

elegans, and was shown to interact genetically with EGL-30 (*C. elegans* Gαq) (Miller et al., 2000). Nematoda and vertebrate Ric-8 has GEF activity and positively regulates HGP signaling *in vivo* and *in vitro* (Afshar et al., 2004; Gabay et al., 2011; Tall et al., 2003). In *Drosophila*, Ric-8 is essential for targeting of HGPs toward the plasma membrane and participates in HGP-dependent processes such as asymmetric division of neuroblasts (David et al., 2005; Hampoelz et al., 2005; Wang et al., 2005).

In this study, we examined the precise role of *ric-8* in mesoderm invagination. We found that cortical stability of ventral cells is impaired in a *ric-8* mutant. By a combination of genetic and pharmacological analyses, we found that blebbing of ventral cells is induced by either disruption of cortical actin or mutation of *ric-8*. We suggest that HGP signaling constitutively organises cortical actin, thereby reinforcing the resistance of cells against deformation.

2. Results

2.1. *ric-8* suppresses blebbing in ventral cells

To examine the function of *ric-8* during gastrulation, we produced female flies harbouring a *ric-8* germ line clone and used their progeny as the *ric-8* mutant. Thus, the maternal contribution of *ric-8* products was avoided. We observed the surface morphology of the *ric-8* mutants by scanning electron microscopy (SEM), and thereby found numerous blebs on their ventral tissue (Fig. 1C and D). The blebs were spherical, and protruded onto the apical part of the tissue. Interestingly, blebs clearly became larger as development proceeded: blebs were massively enlarged during furrow internalisation, and covered the ventral furrow (Fig. 1 E-J). Such apically protruding blebs were not observed in the lateral or dorsal regions of the *ric-8* mutant embryos (Fig. 1D arrow), or in any regions of the wild-type embryos (Fig. 1C). Immuno-fluorescence imaging of transverse sections confirmed that blebs were formed at the apical tip of ventral cells without impairing baso-lateral morphology or cellular conjunction (Fig. 1K and L). Since the enlargement of blebs has not been reported in *ric-8* or other mutants defective for gastrulation, our observations imply that Ric-8 plays some additional role that has been unknown until now.

Given that bleb formation is initiated by detachment of the plasma membrane from cortical actin (Charras et al., 2005), we analysed the pattern of F-actin in live embryos by monitoring the expression of a conventional marker for F-actin, GFP-Moesin (Edwards et al., 1997, Kiehart et al., 2000). In wild-type embryos,

GFP-Moesin was primarily accumulated on the border of blastoderm cells (Fig. 2A). Though the *ric-8* mutant displayed some signals of GFP at cellular borders, a large fraction of the signal was dispersed to the cytoplasm as compared with the wild type (Fig. 2B and C). This abnormal pattern of F-actin localisation was observed not only in ventral cells but also in most if not all cells in the *ric-8* mutant (Fig. 2E, arrow and data not shown). These results indicate that *ric-8* is ubiquitously involved in the organisation of cortical actin throughout the embryo.

Next we observed the surface dynamics of ventral cells by time-lapse imaging using laser confocal microscopy (Movie 1 and 2). Blebs in the *ric-8* mutant were observed by adjusting confocal sections to the most apical level (Fig. 2E). Blebs could be detected when the cells started to take part in the furrow internalisation. These blebs dynamically expanded and shrunk, with a cycle of 30-60 sec (Fig. 2F and Movie 3). Interestingly, some of the blebs became over-expanded and subsequently failed to shrink, and the enclosure of ventral tissue was frequently prevented in the later stage (Fig. 2E; right panel).

2.2. Cortical actin is controlled by HGP

As previously suggested (Hampoelz et al., 2005), ventral cells in the *ric-8* mutant showed uncoordinated apical constriction (Fig. S1A and B, and Movie 1 and 2). During the apical constriction stage, MyoII was not evenly accumulated at the apical surface of ventral cells in the *ric-8* mutant (Fig. 3A and B), though some punctate accumulations were observed. DE-Cadherin in ventral cells did not properly move to the apical surface in the *ric-8* mutant (Fig S2). All of these

phenotypes are hallmarks of impaired Fog-Cta signaling (Dawes-Hoang et al., 2005). To confirm the role of Ric-8 in Fog-Cta signaling, we utilised the *fog* transgene driven by a heat shock promoter (P{*hsfog*}; Morize et al., 1998). When P{*hsfog*} embryos were incubated at 37°C, expression of Fog was ectopically induced and MyoII was localised apically in all cells on the surface of the embryo (Fig. 3C and D). However, the ectopic expression of Fog from P{*hsfog*} failed to cause such apical localization of MyoII under the *ric-8* mutant background (Fig. 3E). These results indicate that Ric-8 is essential for Fog-Cta signaling.

To examine the localization of Cta protein in the *ric-8* mutant, we made an antibody against Cta (see Experimental procedures). The *ric-8* mutant failed in the membrane targeting of Cta as well as all of the HGP proteins we examined (Gα49B, G-iα65A and Gβ13F) (Fig S3A-H; David et al., 2005; Hampoelz et al., 2005; Wang et al., 2005). These results indicate that HGP activity in the *ric-8* mutant is generally compromised, since the membrane localization of HGP is essential for its signaling in developmental and physiological contexts (Marrari et al., 2007).

Next we investigated the function of HGP in the organisation of cortical actin using GFP-Moesin. We found that blastoderm embryos mutated for Cta or G-iα65A exhibit a scattered pattern of GFP-Moesin, similar to that seen in the *ric-8* mutant (Fig. 4A-C). However, GFP-Moesin in ventral cells of the *fog* mutant showed normal distribution (Fig. 4D). This result suggests that the Fog-Cta pathway is involved in apical constriction but is dispensable for cortical actin organisation.

In spite of the disturbed organisation of cortical actin, the *cta*- and *G-ia65A* mutants did not show large blebs on their ventral surface (Fig. 4E and F), though relatively small blebs were observed in the *G-iα65A* mutant (Fig. 4F). We hypothesised that the enlargement of blebs in the *ric-8* mutant was caused by severe disruption of cortical actin via simultaneous inactivation of at least those two HGP pathways, and possibly other HGP pathways as well. To test this hypothesis, we analysed mutants for Gβ13F and Gγ1, since those proteins are the predominantly expressed Gβ and Gγ subunits in blastoderm embryos, and thus their mutations would presumably result in disruption of multiple HGP pathways. In contrast to the *cta* and *G-ia65A* mutants, the *Gγ1* and *Gβ13F* mutants showed blebs on the ventral surface, and the *Gβ13F* mutant also showed abnormal localisation of cortical actin (Fig. 4G and H, and Fig. S3J).

Taken together, our data indicate that HGP is involved in two pathways in *Drosophila* gastrulation: i) Fog-dependent signaling to control contractile acto-myosin in apical constriction, and ii) Fog-independent organisation of cortical F-actin to suppress blebbing.

2.3. Disruption of cortical actin induces blebbing of constricting cells

To directly examine the relationship between F-actin and the ventral cellular surface, we treated wild-type embryos with increasing concentrations of latrunculin B (lat B), an inhibitor of actin polymerisation, which leads to a reduced F-actin level in a dose-dependent manner (Fig. 5A-D). To investigate the effect of such actin perturbation on the ventral furrow, the surface morphology of

the cells was observed by SEM (Fig. 5E-G). In embryos treated with a moderate level of lat B (10 nM), the ventral surface exhibited numerous blebs on the cells' apical surface (Fig. 5F). In the embryos treated with 100 nM lat B, no blebs were visible, and ventral cells failed to undergo constriction and invagination (Fig. 5G). These results suggest that partial disruption of actin filaments results in the blebbing of ventral cells, as seen in the *ric-8* mutant.

While the treatment with lat B perturbed F-actin throughout the entire blastoderm, blebs were observed exclusively in ventral cells (Fig. 5F). Similarly, though F-actin was disturbed globally in the *ric-8* mutant, blebbing was observed only in ventral cells. Given that blebs are induced by contraction of the cytoskeletal network, we wondered whether blebbing could be induced by ectopic contraction of the cytoskeleton in lateral cells. To answer this question, we took advantage of P{*hsfog*}. When P{*hsfog*} embryos were heat-shocked, ectopic expression of Fog induced flattening of the cellular surface all around the embryo (Fig. 5I), similar to the flattening of the wild-type ventral cells. When these embryos were treated with lat B after the heat shock treatment, the lateral cells formed numerous blebs (Fig. 5J), although the blebs in the lateral cells were smaller than those in the ventral cells. These results indicate that the blebbing is restricted to ventral cells of the lat B-treated embryo, but such blebbing can be physically induced by cytoskeletal contraction and F-actin perturbation in any cell.

2.4. Cytoplasmic pressure induces blebbing

Finally we examined the mechanics underlying the blebbing in ventral cells. As mentioned above, the average size of blebs in the *ric-8* mutant was significantly increased during furrow internalisation (Fig. 6A). A similar increase of bleb-size was observed in lat-B-treated embryos. Since an increase of cellular tension is known to cause enlargement of blebs (Tinevez et al., 2009), we wondered whether the enlargement of blebs is caused by contractile force from acto-myosin. To explore this possibility, we analysed the subcellular localisation of MyoII in the *ric-8* mutant. During apical constriction, *ric-8* ventral cells scarcely showed any accumulation of MyoII in the apical cortex, as described above (Fig. 3A, B). However, MyoII was strongly accumulated in punctate structures at the cortex during furrow internalisation (Fig. 6C). These irregular signals were preferentially located at the base of blebs (Fig. 6C, arrow). Thus, MyoII activity and enhancement of blebbing of ventral cells were correlated with each other. To further examine the force in the cytoplasm, we exposed the blebbing embryos to various osmotic conditions: *ric-8* mutant embryos with permeabilised vitelline membranes were incubated with various concentrations of sorbitol. The frequency of bleb formation and the size of blebs decreased as the concentration of sorbitol increased (Fig. 6D-G), indicating that bleb formation can be suppressed by high external osmotic pressure. This result is consistent with the idea that enlargement of blebs is driven by an increase of hydrostatic pressure in the cytoplasm.

3. Discussion

3.1. Mechanism underlying blebbing in ventral cells

As reported previously, ventral cells intrinsically exhibit a few small blebs during mesoderm invagination (Costa et al., 1993). This indicates that surface contraction during apical constriction induces blebbing even in normal invagination. In this study we found that Ric-8 and HGP signaling are required for suppression of abnormally large blebs, and for the stabilisation of the cortex in invaginating cells. The physical mechanism underlying blebbing has been studied extensively in cultured cells. The contractile force of the acto-myosin network causes an increase of hydrostatic pressure in the cytoplasm, which leads to detachment of the plasma membrane from the cortical actin layer (Charras et al., 2005). The dynamics of blebs observed in *ric-8* ventral cells were similar to those reported in cultured cells in terms of time and size (see Charras et al., 2005), suggesting that the mechanisms underlying blebbing in these two systems are conserved.

The average size of blebs changes as development proceeds: blebs become larger during furrow internalisation. Immuno-fluorescence imaging revealed that MyoII is abnormally accumulated beneath enlarged blebs in the *ric-8* mutant. This correlation suggests that MyoII acts to induce an increase of hydrostatic pressure. Although MyoII is an indispensable factor for apical constriction, its activity can also cause malformation of the cells. How MyoII accumulates abnormally in the *ric-8* mutant remains unclear. We cannot rule out the

possibility that other processes of mesoderm invagination, such as mechanical stress from surrounding cells, also contributes to the enlargement of blebs. During apical constriction, epithelial tissue generates tension along the anterior-posterior axis, and ventral cells undergo constriction in an anisotropic manner (Martin et al., 2010). Similar force may also be generated at the tissue level during furrow internalisation, causing the cells there to be squeezed, and consequently increasing the intracellular pressure. Blebbing in the *ric-8* mutant may be a consequence of abnormal cytoskeletal networks and physical stress acting cell to cell. In normal situations, cells would resist such physical stress and maintain the surface integrity, thereby supporting correct morphogenetic movements.

3.2. Dual role of HGP signaling in mesoderm invagination

Our study demonstrates that HGP signaling has two functions in mesoderm invagination: induction of the apical constriction via MyoII accumulation and maintenance of the cellular surface via organisation of cortical actin. Although Fog is required for apical constriction, F-actin is organised in a Fog-independent manner, suggesting that these two functions are regulated in different ways. *cta* mutants and *G-iα65A* mutants showed similar phenotypes regarding cortical actin, suggesting that these Gα paralogs have overlapping functions. Because the *Drosophila* genome encodes 6 Gα subunits and 5 of them are expressed in early embryos (Kuwar et al., 2008, N.F., unpublished data), we cannot rule out the contribution of Gα paralogs other than Cta and G-iα65A to the suppression of

blebbing. Our finding that *ric-8*, *Gβ13F*, and *Gγ1* mutants showed blebbing, a hallmark of severely disturbed cortical actin, supports the idea that multiple HGP pathways control cortical actin redundantly. However, currently we do not know whether those signaling pathways act on the same downstream effectors. Considering that most blastoderm cells showed a dispersed signal of GFP-Moesin in the mutants, HGPs appear to be rather constitutive regulators of cortical actin organisation. Nevertheless, the abnormality of the cortex does not affect the morphology of the 'standstill' cells that do not carry out the inward movement. Thus, HGPs are required to reinforce the cortex so that the cells can endure the stress generated during tissue folding.

It was previously reported that *ric-8* is required for *Drosophila* gastrulation (Hampoelz et al., 2005). Here, we extensively investigated mesoderm invagination and found that apical constriction is indeed compromised in the *ric-8* mutant. Based on our observation of Fog-dependent MyoII accumulation, we concluded that *ric-8* is required for Fog-Cta signaling. It is unlikely that this phenotype is a secondary consequence of the disorganised F-actin in the *ric-8* mutant, because actin was organised normally in the *fog* mutant embryo and ectopic Fog expression induced cell flattening even in lat B-treated embryos. These findings instead suggested that Fog-Cta signaling and actin organisation are separate pathways and Ric-8 is involved in both pathways.

Given that HGPs constitutively regulate F-actin, the signaling seems to be active in most blastoderm cells. Some unknown extracellular ligand and its receptor thus appear to be expressed to activate HGPs. It is also possible that

cytoplasmic HGP regulators such as Pins, Loco, or other RGS proteins are involved in the activation. In the formation of the blood-brain barrier in *Drosophila,* Pins and Loco positively regulate HGP signaling (Schwabe et al., 2005). Embryos mutant for Pins also show abnormal cellular movements during mesoderm invagination (N. F., unpublished data). It is also intriguing to hypothesise that Ric-8 participates in the activation of HGPs through its GEF activity, which has been characterised both *in vivo* and *in vitro* (Afshar et al., 2004; Gabay et al., 2011; Tall et al., 2003). This hypothesis suggests the possibility that HGPs are endogenously activated. Future analysis of the responsible cytoplasmic regulators may clarify the mechanism of HGP regulation, and may give new insights regarding the intricate network of HGP signaling in animal development.

3.3 Molecular mechanism of cortical actin organisation

How might HGP be functionally linked to actin polymerisation? Since Gα12/13 participates in the activation of Formin family proteins in mammalian fibroblasts (Goulimari et al., 2005) and a human Formin inhibits the formation of blebs in a prostate cancer cell line (Di Vizio et al., 2009), a candidate factor regulating actin filaments downstream of HGP could be Diaphanous (Dia), a *Drosophila* Formin. Although it has been shown that organisation of actin via Dia is required for ventral furrow invagination (Homem and Peifer, 2008), it is unclear whether Dia is also required for cortical stability during morphogenesis. Considering that Dia is an actin nucleator (Afshar et al., 2000), we speculate

that Dia might act in the assembly of the actin meshwork and thereby reinforce the cortex. Indeed, we observed that the *dia* mutant embryos showed cellular deformation during gastrulation (data not shown), suggesting the functional relevance of the actin nucleator in the suppression of blebs. Further analysis will be required to clarify the functions of Dia.

Previous studies demonstrated that ventral cells form a particular type of F-actin meshwork that makes a basic frame for apical constriction (Fox and Peifer, 2007; Martin et al., 2009). RhoA- and Abelson-mediated signaling is required for organisation of the apical F-actin meshwork, while the Fog-Cta pathway is not (Fox and Peifer, 2007). Thus, it is surprising that the mutants for HGPs, including Cta, showed a defect of cortical actin. HGP signaling may organise only a moiety of F-actin which is distinct from the one specifically accumulated at apices. HGP signaling regulates the organisation of cortical actin and mediates the establishment of the blood-brain barrier in *Drosophila* (Schwabe et al., 2005), suggesting that this function of HGPs is rather common in fly embryogenesis.

4. Experimental procedures

4.1. Fly strains

Flies of *yw* background were used as the wild type, unless otherwise stated. The *ric-8* null mutant fly (*ric-8*^{P587}; Wang et al., 2005) was kindly provided by Dr. F. Yu. We confirmed that homo-lethality of *ric-8*^{P587} was rescued by an *hsp83* promoter-driven *ric-8* cDNA construct (data not shown). The following flies were used in this study: *cta*^{RC10}; *fog*^{4a6} (Costa et al., 1994); P{*hsfog*} (Morize et al., 1998); *G-iα65A*^{P8} (Yu et al., 2003); *Gβ13F*$^{\Delta 15}$ (Fuse et al., 2003); *Gγ1*^{N159} (Izumi et al., 2004); *P{sqh–moesinGFP}* sGMCA-3.1 (Kiehart et al., 2000); *P{DE-Cadherin-GFP}* (Oda et al., 1998). Germ line clones for *ric-8*, *G-iα65A, Gβ13F,* and *Gγ1* were made using the FLP-DFS system (Chou and Perrimon, 1992; Chou and Perrimon, 1996). The zygotic genotype of the cloned embryos was determined based on the expression of marker genes on balancer chromosomes, and then the zygotic homozygous mutants were taken as maternal and zygotic mutant embryos.

4.2. Antibodies

Rabbit anti-G-iα65A, rabbit anti-Gα49B, and rabbit anti-Zipper (MyoII heavy chain) were kindly provided by Dr. F. Matsuzaki. Published antibody resources were obtained as follows: mouse anti-DE-Cad (DSHB); rabbit anti-Gβ13F (Fuse et al., 2003); mouse anti-Miranda (Ikeshima-Kataoka et al., 1997); mouse anti-Dlg (DSHB).

Rabbit anti-Cta antibody was made as follows: cDNA encoding full-length Cta was subcloned into the multi-cloning site of pQE80E vector (Qiagen) in frame. *E. coli* BL21 cells transformed with this construct were cultured and treated with 1 mM IPTG. The recombinant protein was purified from the cell lysate with Ni-NTA resin (Qiagen) in denaturing conditions according to the manufacturer's protocol. After dialysis, the protein solution was used as antigen. After injection and preparation of antiserum performed by MBL Co., Japan, the Cta antibody was affinity-purified with the antigen, according to the standard protocol (Harlow and Lane, 1988). The specificity of the antibody was tested by immuno-staining of embryos and by western blotting of lysates of embryos and cultured cells (Fig. S4). To prepare Cta-expressing cells, *Drosophila* S2 cells (Invitrogen) were transfected with pW8-actin5c-Gal4 (from Dr. Y. Hiromi) and pUAST-cta constructs using a Calcium Phosphate Transfection Kit (Invitrogen). Cell lysates were prepared using the standard protocol (Harlow and Lane, 1988).

4.3. Immuno-staining and confocal imaging

Embryos were washed, dechorionated, and fixed by vigourously shaking in fixation solution (1:1 solution of 4% formaldehyde-PBS and heptane) for 20 min. After devitellinization in methanol or 80% ethanol (for phalloidin staining), embryos were rinsed with PBST (PBS containing 0.2% Tween 20) three times, and incubated with blocking solution (PBST containing 1% skim-milk or 0.2% BSA) for 2 hr at room temperature. Embryos were then incubated with primary antibody in blocking solution for 2 hr at room temperature. After washing with

PBST three times, embryos were incubated with secondary antibody for 2 hr at room temperature, washed with PBST three times, and mounted in Vectashield (Vector Laboratories) for microscopy. For observing transverse sections, embryos were sliced by hand using a surgical knife after immuno-staining. Primary antibody was diluted in blocking solution as follows: anti-Zipper 1:400, anti-Gαi65A 1:100, anti-Cta 1:50, anti-Gα49B 1:50, anti-Gβ13F 1:2000, anti-Mir 1:50, anti-DE-Cad 1:20 and anti-Dlg 1:20. For phalloidin staining, 1:50 diluted Alexa568-Phalloidin (Molecular Probes) was used.

Confocal images of immuno-stained embryos were obtained using a Carl Zeiss LSM5 LIVE or LSM510 META system. Image analyses were performed using LSM Image Browser (Carl Zeiss) and ImageJ (NIH, USA; http://rsbweb.nih.gov/ij/). In all of our experiments, images for each combination of wild type and mutant were obtained with the same brightness and contrast. Time-lapse imaging was carried out according to the method of Kato et al., 2004.

Quantification of GFP-Moesin signals was performed using the raw confocal images. For each measurement, we quantified 50 pixels (~5.5 μm) of linear region across the cellular border. The relative intensity (RI*i*) was calculated using $RIi = (Ii - I_{min}) / (I_{max} - I_{min}) \times 100$, where I*i* is absolute intensity of GFP at the *i*th pixel, and I_{max} and I_{min} are the maximal- and the minimal intensity in the image of the embryo, respectively.

4.4. SEM imaging

The embryos were fixed, devitellinized, and stained for chromosomal markers so that the zygotic genotype could be determined. Embryos with the desired genotype were collected under a microscope and fixed again with 25% glutaraldehyde for 30 min at room temperature. Fixed embryos were washed in PBST three times, and incubated with 30, 60, 90, and 99.5% EtOH each for 30 min. After washing with t-butanol three times, embryos were freeze-dried and ion-coated. SEM imaging was carried out with JEOL JSM-5800LV. The diameter of blebs (widest diameter of the hemisphere) in wild-type embryos treated with lat B and in *ric-8* embryos was measured from SEM images. The measurement was done using analysis functions in ImageJ. Statistical significance of variations in bleb sizes was examined by Student's t-test, using R programming environment (http://www.r-project.org/).

4.5. Toxin- and heat shock-treatment of embryos

Lat B treatment of wild-type embryos was carried out as follows. Dechorionated embryos were gently shaken in a 1:1 mixture of *n*-octane and Schneider's medium (Gibco) containing various concentrations of lat B for 15 min at room temperature. After the incubation, the embryos were fixed and then observed with the imaging method described above.

Heat-shock treatment of P{*hsfog*} embryos was carried out as follows. 2-4 hr AEL (after egg laying) embryos were collected, washed, and incubated in a 37°C water bath for 10 min. Afterwards the embryos were transferred into a 25°C water bath and incubated for 20 min. The embryos were fixed and immuno-

stained for Zipper protein.

4.6. Sorbitol treatment

The sorbitol-treatment experiment was designed according to previously reported experiments (Fedier and Keller, 1998; Charras et al., 2005). Dechorionated embryos were gently shaken in a 1:1 mixture of *n*-octane and Schneider's medium (Gibco) containing various concentrations of sorbitol for 10 min at room temperature. After the incubation, the embryos were fixed, washed, and ion-coated for SEM imaging. Only embryos at the furrow internalisation stage were used for imaging and counting. The embryos were sorted into three classes according to the severity of deformation of their ventral surface (See legend for Fig. 6), and then the number of the embryos in each class was counted. Proportions of the classified embryos were statistically examined using Pearson's Chi-squared test with R programming environment.

Figure legends

Fig. 1. *ric-8* mutation results in blebbing of ventral cells.

(A, B) Mesoderm invagination in *Drosophila melanogaster*. Wild-type embryos in the apical constriction- (A) and furrow invagination (B) stages were stained with anti-DE-Cadherin antibody (magenta) and DAPI (green). Ventral furrow is indicated by arrowhead. Ventral is toward the bottom. (C and D) Surface morphology of wild type- (C) and *ric-8* (D) embryos was observed by SEM. Numerous blebs were observed in the ventral cells (arrowhead) but not in the lateral cells (arrow) of *ric-8* embryos. Anterior is toward the left. (E-J) Magnified images of wild-type (E-G) and *ric-8* (H-J) ventral cells during apical constriction (E and H), furrow internalisation (F and I), and the terminal period of mesoderm invagination (G and J). Anterior is toward the top. (K and L) Transverse section of wild-type (K) and *ric-8* (L) embryos stained for a membrane-associated protein, Discs large. Apical (ventral) is toward the top. Blebs were formed at the apical surface of the *ric-8* ventral cells (arrows). Scale bars; (B, D), (J) 10 μm, (L) 20 μm.

Fig. 2. *ric-8* phenotype in live embryos.

(A and B) Sub-apical section of blastoderm cells expressing GFP-Moesin in wild-type (A) and *ric-8* (B) embryos. (C) Quantitative analysis of GFP-Moesin distribution. The distribution of the GFP signal across the cellular border was quantified from the confocal images of wild type- (blue) and *ric-8* (yellow) embryos. Relative GFP intensity and standard deviation (n=20 for each

genotype) was plotted versus distance. The (D) wild-type and (E) *ric-8* ventral surface was visualised with GFP-Moesin and observed by time-lapse imaging analyses. Time after initiation of apical constriction is shown at the top of the images. GFP-Moesin was dispersed in most cells including ventral (arrow head) and lateral (arrow) cells of *ric-8* embryos. Anterior is toward the upper left (D) or the left (E). (F) Highly magnified time-lapse images of blebs in *ric-8* embryo. Blebs dynamically expanded and shrunk (arrows). Scale bars; (B, D, E) 10 μm, (F) 20 μm.

Fig. 3. Fog-Cta signaling is compromised in the *ric-8* mutant.
(A, B) Wild type- and *ric-8* embryos at the apical constriction stage were stained for Zipper (MyoII heavy chain), and their ventral side was observed. (C-E) Effect of ectopic Fog expression. Wild-type (C), P{*hsfog*}/+ (D), and *ric-8*; P{*hsfog*}/+ (E) embryos were heat-shocked, and MyoII distribution was observed in lateral cells. Arrows indicate the apical accumulation of Zipper induced by Fog-Cta signaling. Scale bars; 20 μm.

Fig. 4. HGP signaling is required for organisation of cortical actin.
(A-D) GFP-Moesin distribution in blastoderm cells in wild-type (A), *G-iα65A* (B), *cta* (C), and *fog* (D) embryos. (E-H) Ventral cellular morphology in *cta* (E), *G-iα65A* (F), *Gβ13F* (G), and *Gγ1* (H) embryos. Scale bars; 10 μm.

Fig. 5. The induction of blebs in lat B-treated embryos.

(A-D) Wild-type embryos incubated with lat B-containing medium were fixed and stained with phalloidin (for F-actin), and their blastoderm cells were observed by confocal microscopy. The embryos were treated with 0, 20, 40, or 60 nM lat B (from panel A to panel D, respectively). (E-G) SEM images of the ventral surface in wild-type embryos treated with 0 nM (E), 10 nM (F), or 100 nM (G) lat B. Anterior is toward the top. (H-J) P{*hsfog*} embryos were treated with 10 nM lat B (H), heat shock (I), or both (J), and their lateral surface morphology was observed by SEM. The arrows indicate small blebs at lateral cells. Scale bars; 10 μm.

Fig. 6. Cytoplasmic pressure induces blebs.

(A) The average diameter of blebs in wild-type embryos treated with lat B and in *ric-8* embryos. For each genotype, apical constriction (AC)- and furrow internalisation (FI) stages of embryos were investigated. For each stage, more than 60 blebs from 3 embryos were observed. *** indicates statistical significance (p-value < 0.001, Student's t-test). (B, C) MyoII distribution during furrow internalisation stage in wild-type (B) and *ric-8* (C) embryos. Apical (ventral) is toward the top. (D-F) *ric-8* embryos were treated with sorbitol, and according to the number and size of blebs, embryos were categorized into the following three class of phenotype: Class I, whole ventral furrow is filled with many large blebs and the furrow fails to be closed (D); class II, many blebs are formed but the ventral furrow ingresses inward (conventional *ric-8* phenotype) (E); class III, blebs are smaller and many cells show normal surface morphology

(F). Anterior is toward the top. (G) Sorbitol treatment suppresses bleb formation in *ric-8* mutant. The proportions of the embryos in class I-III are indicated, and a statistically significant difference was detected between the control and 1 M sorbitol-treatment (p-value < 0.05, Pearson's Chi-squared test). The number of embryos counted for each individual condition was 81 (0 M, control), 86 (0.5 M sortbitol-treatment), and 78 (1 M sortbitol-treatment). Scale bar; 20 μm.

Acknowledgements

We thank Drs F. Yu, F. Matsuzaki, S. Hayashi, H. Oda, Y. Hiromi, and E. Wieschaus for providing materials, Dr. Y. Hiromi and colleagues of NIG for suggestions and discussions, and Dr. E. Nakajima for critical reading of the manuscript. We also thank Kyoto Drosophila Genetics Resource Center, Bloomington Drosophila Stock Center, The Developmental Studies Hybridoma Bank, and The Drosophila Genomics Resource Center for providing us fly strains, antibodies and DNA constructs. This work was supported by a Grant-in-Aid for Science Research from the Ministry of Education, Science, Culture and Sports of Japan.

References

Afshar, K., Stuart, B., Wasserman, S.A., 2000. Functional analysis of Drosophila diaphanous FH protein in early embryonic development. Development 127, 1887-1897.

Afshar, K., Willard, F.S., Colombo, K., Johnston, C.A., McCudden, C.R., Siderovski, D.P., 2004. RIC-8 is required for GPR-1/2-dependent Gα function during asymmetric division of C. elegans embryos. Cell 119, 219-230.

Blaser, H., Reichman-Fried, M., Castanon, I., Dumstrei, K., Marlow, F.L., Kawakami, K., 2006. Migration of zebrafish primordial germ cells: a role for myosin contraction and cytoplasmic flow. Dev. Cell 11, 613-627.

Charras, G.T., Yarrow, J.C., Horton, M.A., Mahadevan, L., Mitchison, T.J., 2005. Non-equilibration of hydrostatic pressure in blebbing cells. Nature 435, 365-369.

Chou, T.B., Perrimon, N., 1992. Use of a yeast site-specific recombinase to produce female germline chimeras in Drosophila. Genetics 131, 643-653.

Chou, T.B., Perrimon, N., 1996. The autosomal FLP-DFS technique for generating germline mosaics in Drosophila melanogaster. Genetics 144, 1673-1679.

Costa M., Sweeton, D., Wieschaus E., 1993. Gastrulation in Drosophila: cellular mechanisms of morphogenetic movements. In Bate, M., Martinez-Arias,A. (eds), The Development of Drosophila. Cold Spring Harbor Laboratory Press, Cold Spring Harbor, NY, pp. 425–466.

Costa, M., Wilson, E., Wieschaus, E., 1994. A putative cell signal encoded by the

folded gastrulation gene coordinates cell shape changes during Drosophila gastrulation. Cell 76, 1075-1089.

David, N.B., Martin, C.A., Segalen, M., Rosenfeld, F., Schweisguth, F., Bellaiche, Y., 2005. Drosophila Ric-8 regulates Gαi cortical localisation to promote Gαi-dependent planar orientation of the mitotic spindle during asymmetric cell division. Nat. Cell Biol. 7, 1083-1090.

Dawes-Hoang, R., Parmar, K., Christiansen, A., Phelps, C., Brand, A., Wieschaus, E., 2005. folded gastrulation, cell shape change and the control of myosin localisation. Development 132, 4165-4178.

Di Vizio, D., Kim, J., Hager, M.H., Morello, M., Yang, W., Lafargue, C.J., Freeman, M.R., 2009. Oncosome formation in prostate cancer: association with a region of frequent chromosomal deletion in metastatic disease. Cancer Res. 69, 5601-5609

Edwards, K.A., Demsky, M., Montague, R.A., Weymouth, N., Kiehart, D. P., 1997. GFP-moesin illuminates actin cytoskeleton dynamics in living tissue and demonstrates cell shape changes during morphogenesis in Drosophila. Dev Biol. 191,103-117.

Fackler, O.T., Grosse, R., 2008. Cell motility through plasma membrane blebbing. J. Cell Biol. 181, 879-884.

Fedier A, Keller HU., 1997. Suppression of bleb formation, locomotion, and polarity of Walker carcinosarcoma cells by hypertonic media correlates with cell volume reduction but not with changes in the F-actin content. Cell Motil. Cyto. 37, 326-337.

Fox, D.T., Peifer, M., 2007. Abelson kinase (Abl) and RhoGEF2 regulate actin organisation during cell constriction in Drosophila. Development 134, 567-578.

Fuse, N., Hisata, K., Katzen, A.L., Matsuzaki, F., 2003. Heterotrimeric G proteins regulate daughter cell size asymmetry in Drosophila neuroblast divisions. Curr. Biol. 13, 947-954.

Gabay, M., Pinter, M.E., Wright, F.A., Chan, P., Murphy, A.J., Valenzuela, D.M., Yancopoulos, G.D., Tall, G.G., 2011. Ric-8 proteins are molecular chaperones that direct nascent G protein α subunit membrane association. Sci Signal. 4, ra79.

Goulimari, P., Kitzing T.M., Knieling H., Brandt, D.T., Offermanns, S., Grosse, R., 2005. Galpha12/13 is essential for directed cell migration and localiyed Rho-Dia1 function. J. Biol. Chem. 280, 42242-42251.

Hampoelz, B., Hoeller, O., Bowman, S.K., Dunican, D., Knoblich, J.A., 2005. Drosophila Ric-8 is essential for plasma-membrane localisation of heterotrimeric G proteins. Nat. Cell Biol. 7, 1099-1105.

Harlow, E., Lane, D., 1988. Antibodies; A laboratory manual. Cold Spring Harbor Laboratory Press, New York.

Homem, C.C., Peifer, M., 2008. Diaphanous regulates myosin and adherens junctions to control cell contractility and protrusive behavior during morphogenesis. Development 135, 1005-1018.

Ikeshima-Kataoka, H., Skeath, J.B., Nabeshima, Y., Doe, C.Q., Matsuzaki, F., 1997. Miranda directs Prospero to a daughter cell during Drosophila asymmetric divisions. Nature 390, 625-629.

Izumi, Y., Ohta, N., Itoh-Furuya, A., Fuse, N., Matsuzaki, F., 2004. Differential

functions of G protein and Baz-aPKC signaling pathways in Drosophila neuroblast asymmetric division. J. Cell Biol. 164, 729-738

Kardash, E., Reichman-Fried, M., Maitre, J., Boldajipour, B., Papusheva, E., Messerschmidt, E., 2010. A role for Rho GTPases and cell-cell adhesion in single-cell motility in vivo. Nat. Cell Biol. 12, 47-53.

Kato, K., Chihara, T., Hayashi, S., 2004. Hedgehog and Decapentaplegic instruct polarized growth of cell extensions in the Drosophila trachea. Development 131, 5253-5261.

Kunwar, P.S., Sano, H., Renault, A.D., Barbosa, V., Fuse, N., Lehmann, R., 2008. Tre1 GPCR initiates germ cell transepithelial migration by regulating Drosophila melanogaster E-cadherin. J Cell Biol. 183, 157-168.

Kiehart, D.P., Galbraith, C.G., Edwards, K.A., Rickoll, W.L., Montague, R.A., 2000. Multiple forces contribute to cell sheet morphogenesis for dorsal closure in Drosophila. J Cell Biol. 149, 471-479.

Lecuit, T., Lenne, P.F., 2007. Cell surface mechanics and the control of cell shape, tissue patterns and morphogenesis. Nature Rev. Mol. Cell Biol. 8, 633-644.

Marrari Y., Crouthamel M., Irannejad R., Wedegaertner P.B., 2007. Assembly and Trafficking of Heterotrimeric G Proteins. Biochemistry 46, 7665–7677.

Martin, A. C., Gelbart, M., Fernandez-Gonzalez, R., Kaschube, M., Wieschaus, E. F., 2010. Integration of contractile forces during tissue invagination. J. Cell Biol. 188, 735-749.

Martin, A., Kaschube, M., Wieschaus, E., 2009. Pulsed contractions of an actin-myosin network drive apical constriction. Nature 457, 495-499.

Morize, P., Christiansen, A., Costa, M., Parks, S., Wieschaus, E., 1998. Hyperactivation of the folded gastrulation pathway induces specific cell shape changes. Development 125, 589-597.

Oda H., Tsukita, S., Takeichi, M., 1998. Dynamic Behavior of the Cadherin-Based Cell–Cell Adhesion System during *Drosophila* Gastrulation. J. Cell Sci. 203, 435-450.

Parks, S., Wieschaus, E. 1991. The Drosophila gastrulation gene concertina encodes a Gα-like protein. Cell 64, 447-458.

Schwabe, T., Bainton, R. J., Fetter, R.D., Heberlein, U., Gaul, U., 2005. GPCR signalling is required for blood-brain barrier formation in Drosophila. Cell 123, 133-144.

Sweeton, D., Parks, S., Costa, M., Wieschaus, E., 1991. Gastrulation in Drosophila: the formation of the ventral furrow and posterior midgut invaginations. Development 112, 775-789.

Tall, G.G., Krumins, A.M., Gilman, A.G., 2003. Mammalian Ric-8A (synembryn) is a heterotrimeric Gα protein guanine nucleotide exchange factor. J. Biol. Chem. 278, 8356-8362.

Tinevez, J.Y., Schulze, U., Salbreux, G., Roensch, J., Joanny, J.F., Paluch, E., 2009. Role of cortical tension in bleb growth. Proc. Nat. Acad. Sci. 106, 18581-18586.

Wang, H., Ng, K.H., Qian, H., Siderovski, D.P., Chia, W., Yu, F., 2005. Ric-8 controls Drosophila neural progenitor asymmetric division by regulating heterotrimeric G proteins. Nat. Cell. Biol. 7, 1091-1098.

Yu, F., Cai, Y., Kaushik, R., Yang, X., Chia, W., 2003. Distinct roles of Gαi and Gβ13F subunits of the heterotrimeric G protein complex in the mediation of Drosophila neuroblast asymmetric divisions. J. Cell Biol. 162, 623-633.

Supplementary figures

Fig. S1 Abnormal movement of ventral tissue in the *ric-8* mutant.
(A and B) Ventral cellular movements in wild-type (A) and *ric-8* (B) embryos were observed by time-lapse imaging analyses. The extent of dispersion of GFP-Moesin in the *ric-8* mutant is dependent on the apico-basal position and the embryonic stage. It is more severe at apical positions and at late stages. The GFP-Moesin images were obtained from an inside z-section (about 7 μm depth from embryo). The movement of some cells was traced and marked using the following color code: cells on the ventral midline (blue), cells laterally located at 2 cell-widths (yellow) or 8 cell-widths (red) away from the midline. Scale bars; 10 μm

Fig. S2. Proteins driving apical constriction are mislocalised in *ric-8* mutant.
Wild-type (A, C, E) and *ric-8* (B, D, F) embryos were stained for MyoII (green) and DE-Cad (magenta). Individual images were obtained from embryos during pre-gastrulation (A, B), apical constriction (C, D), and furrow internalisation (E, F) stages. Scale bar; 20 μm.

Fig. S3 *ric-8* is required for HGP targeting.
(A-B'') each wild-type or *ric-8* gastrula-stage embryo was co-stained for Cta (A, B) and Miranda (cellular cortex marker: A', B'), and their co-localisation was examined (A'' and B''). (C-H) wild-type and *ric-8* embryos were stained for G-

iα65A (C, F), Gα49B (D, G), or Gβ13F (E, H). (I, J) Moesin-GFP distribution was observed in wild-type (I) and *Gβ13F* mutant (J) gastrulae embryos. Scale bars; 10 μm.

Fig. S4　Specificity of Cta antibody

(A) Western blots of lysates of S2 cultured cells with anti-Cta antibody. Anti-Cta antibody stained two bands around 50 kD in cells transfected with actin-Gal4 and UAS-cta constructs (actin > cta), but not in control cells. These bands closely correspond to the molecular mass of Cta protein (52 kD), and one of them might correspond to a form of the Cta protein modified or processed in S2 cells. Numbers on the right indicate the molecular mass of size markers. (B) Western blots of embryonic lysates with anti-Cta antibody. Anti-Cta antibody detected one band around 50 kD, which closely corresponded to the size of the lower band detected in S2 cells. Cta protein is larger than other Gα proteins (41-46 kD), suggesting that this antibody recognizes Cta protein specifically. The lysate of the cta^{RC10} mutant embryos also showed one band, corresponding to the wild-type band. (C, D) High magnification views of embryos stained with anti-Cta antibody. Immuno-staining signals were localized at the cell cortex in the wild-type embryo (C), but were diffused to the cytoplasm in the cta^{RC10} mutant embryo (D). These results suggest that the cta^{RC10} mutant is not protein null, but rather might be a missense mutant. Scale bar; 10 μm.

Movie 1. Dynamics of ventral tissue in a wild-type embryo expressing GFP-Moesin during ventral furrow invagination. Scale bar; 10 μ m.

Movie 2. Dynamics of ventral tissue in a *ric-8* mutant expressing GFP-Moesin during ventral furrow invagination. Scale bar; 10 μ m.

Movie 3. The blebbing of ventral cells in *ric-8* mutant expressing GFP-Moesin. Note that the surface of invaginating cells shows continuous expansion and shrinkage of blebs. Scale bar; 10 μ m.

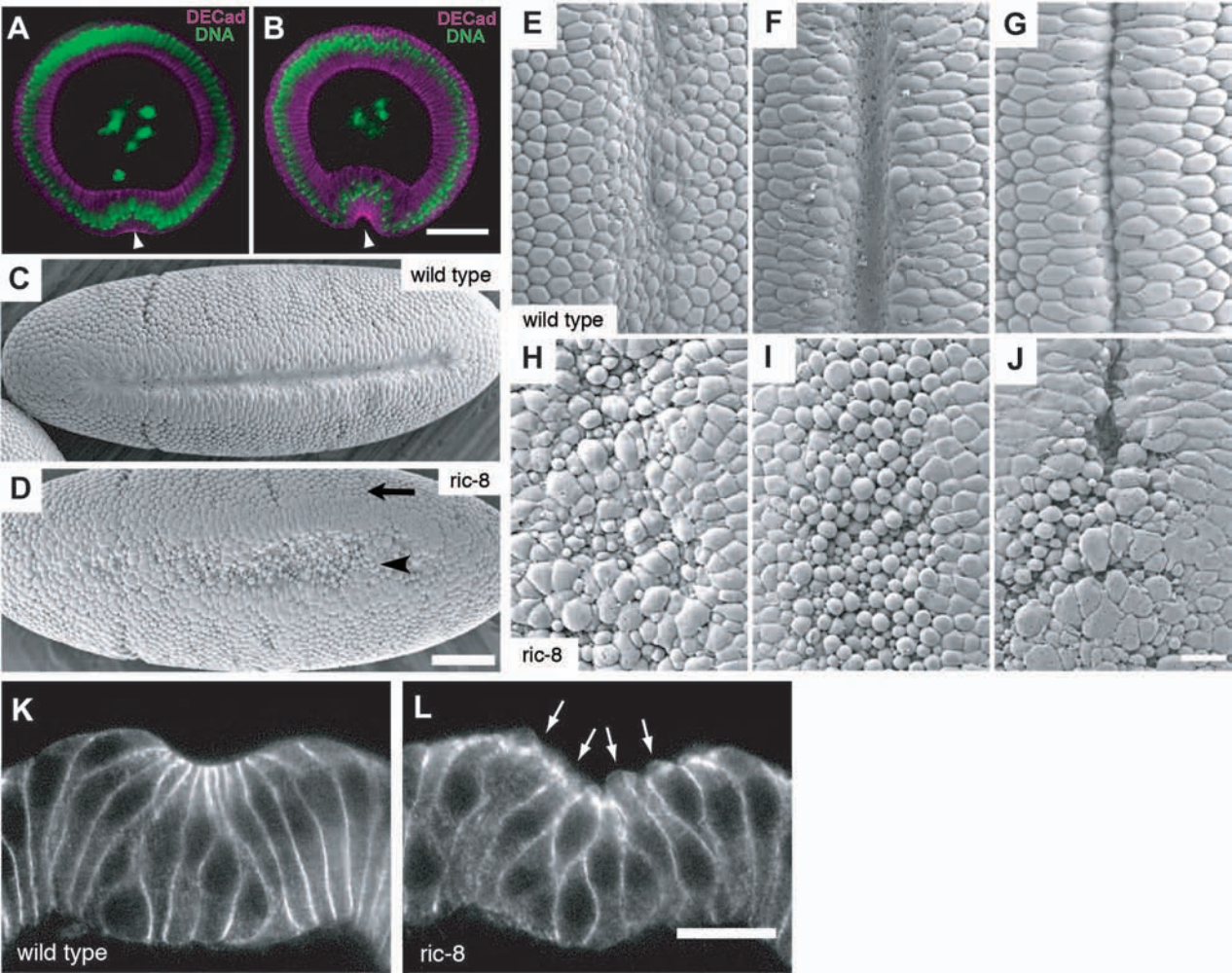
A
DECad
DNA
B
DECad
DNA
C
wild type
D
ric-8
E
wild type
F
G
H
ric-8
I
J
K
wild type
L
ric-8

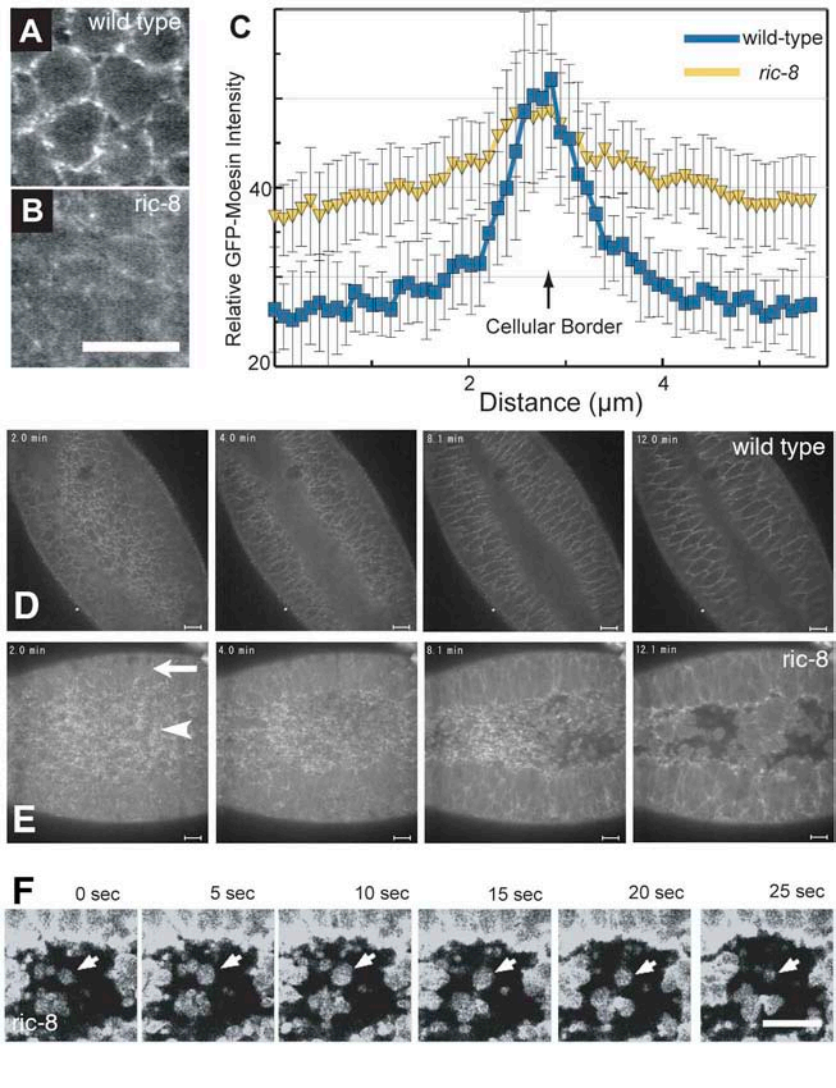
A
wild type
B
ric-8
C
wild-type
ric-8
Relative GFP-Moesin Intensity
40
20
Cellular Border
2
4
Distance (μm)
D
2.0 min
4.0 min
8.1 min
12.0 min
wild type
E
2.0 min
4.0 min
8.1 min
12.1 min
ric-8
F
0 sec
5 sec
10 sec
15 sec
20 sec
25 sec
ric-8

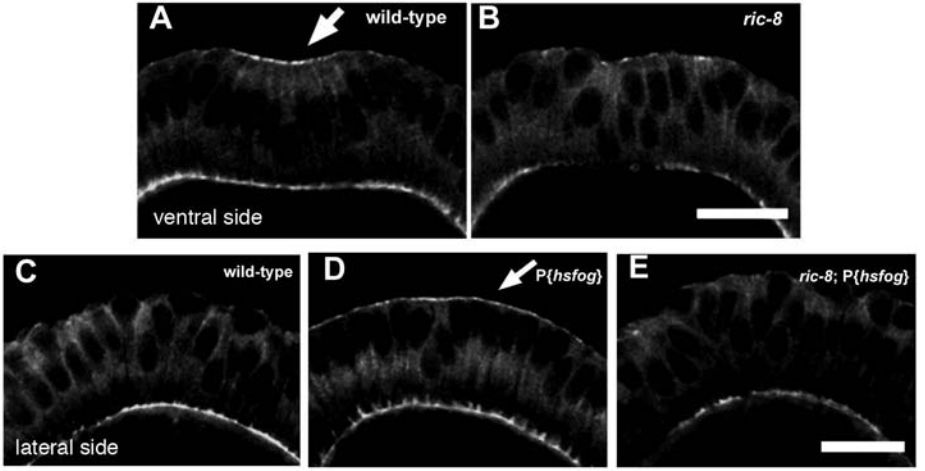
A
wild-type
B
ric-8
ventral side
C
wild-type
D
P{hsfog}
E
ric-8; P{hsfog}
lateral side

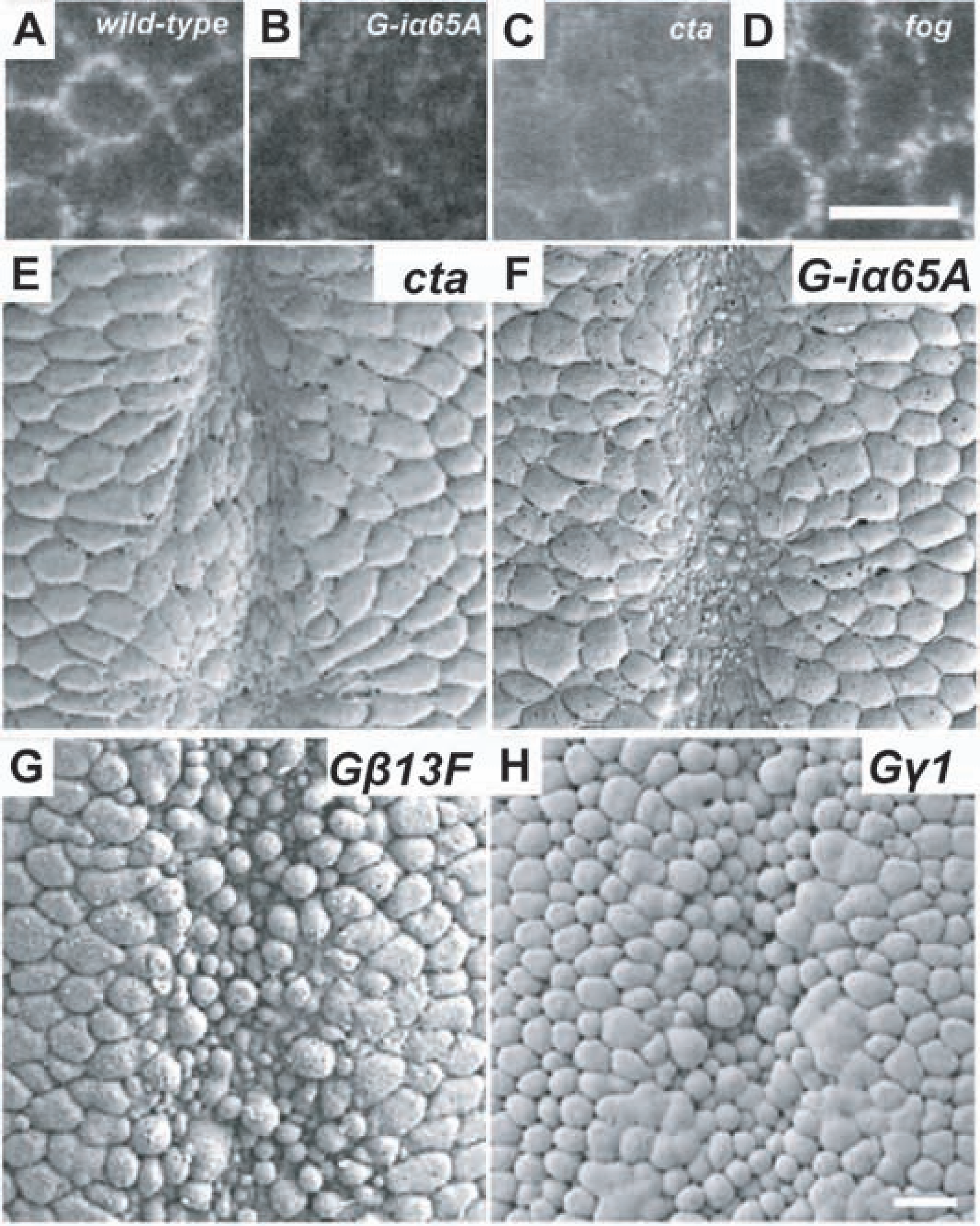
A
wild-type
B
G-iα65A
C
cta
D
fog
E
cta
F
G-iα65A
G
Gβ13F
H
Gγ1

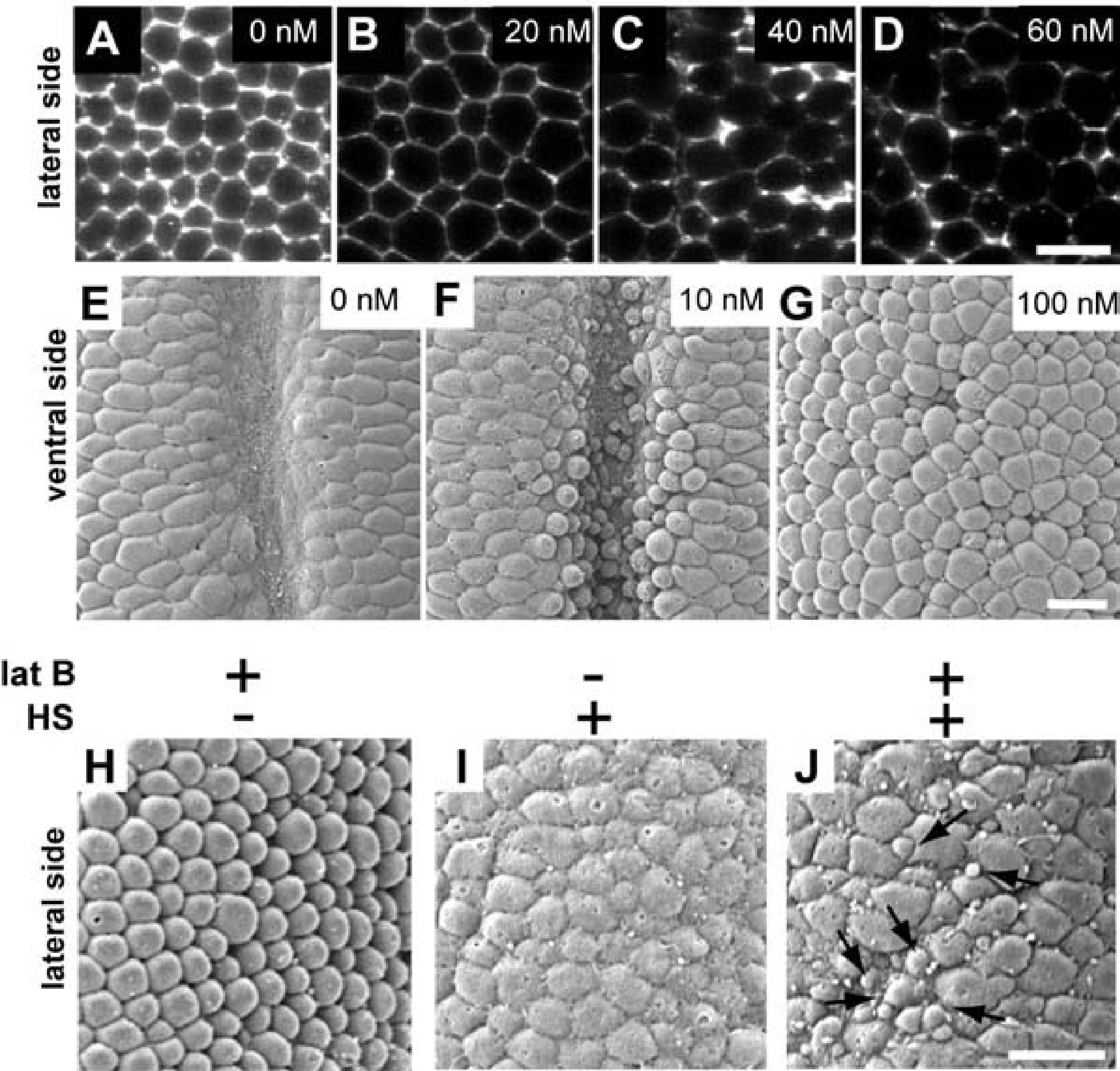
A
0 nM
B
20 nM
C
40 nM
D
60 nM
lateral side
E
0 nM
F
10 nM
G
100 nM
ventral side
lat B
HS
+
-
-
+
+
+
H
I
J
lateral side

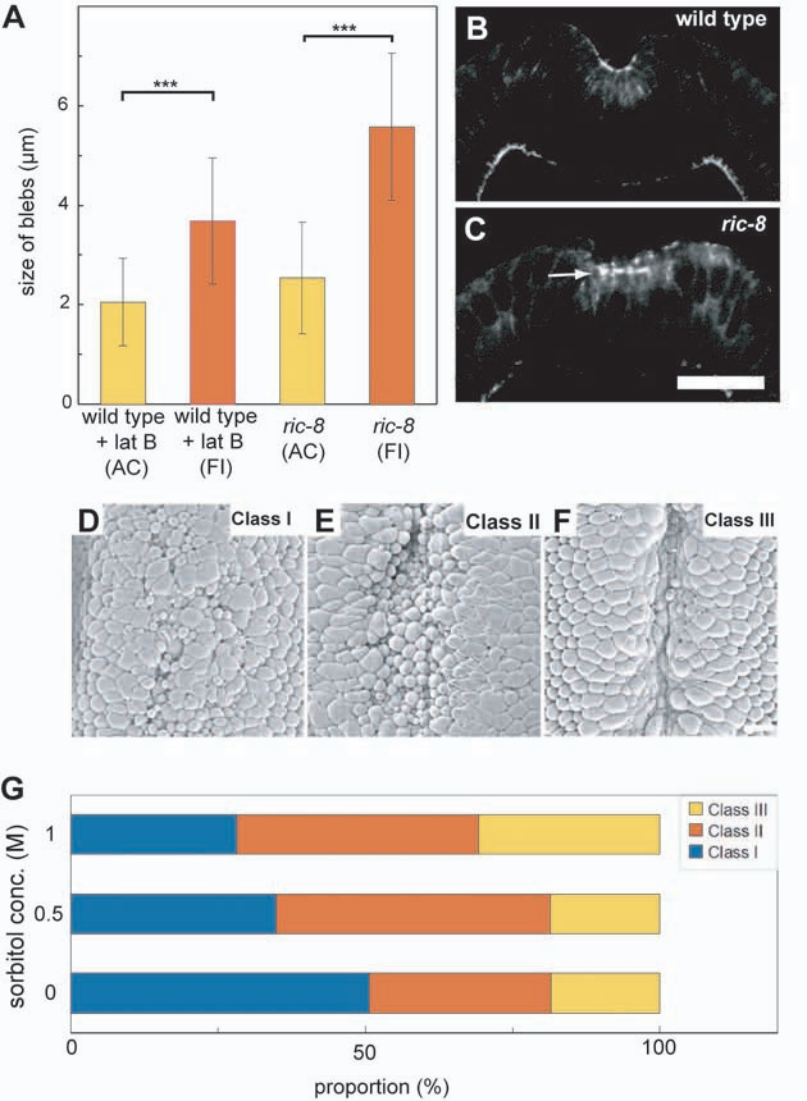
A
size of blebs (µm)
0
2
4
6
***
***
wild type + lat B (AC)
wild type + lat B (FI)
ric-8 (AC)
ric-8 (FI)
B
wild type
C
ric-8
D
Class I
E
Class II
F
Class III
G
sorbitol conc. (M)
1
0.5
0
Class III
Class II
Class I
0
50
100
proportion (%)

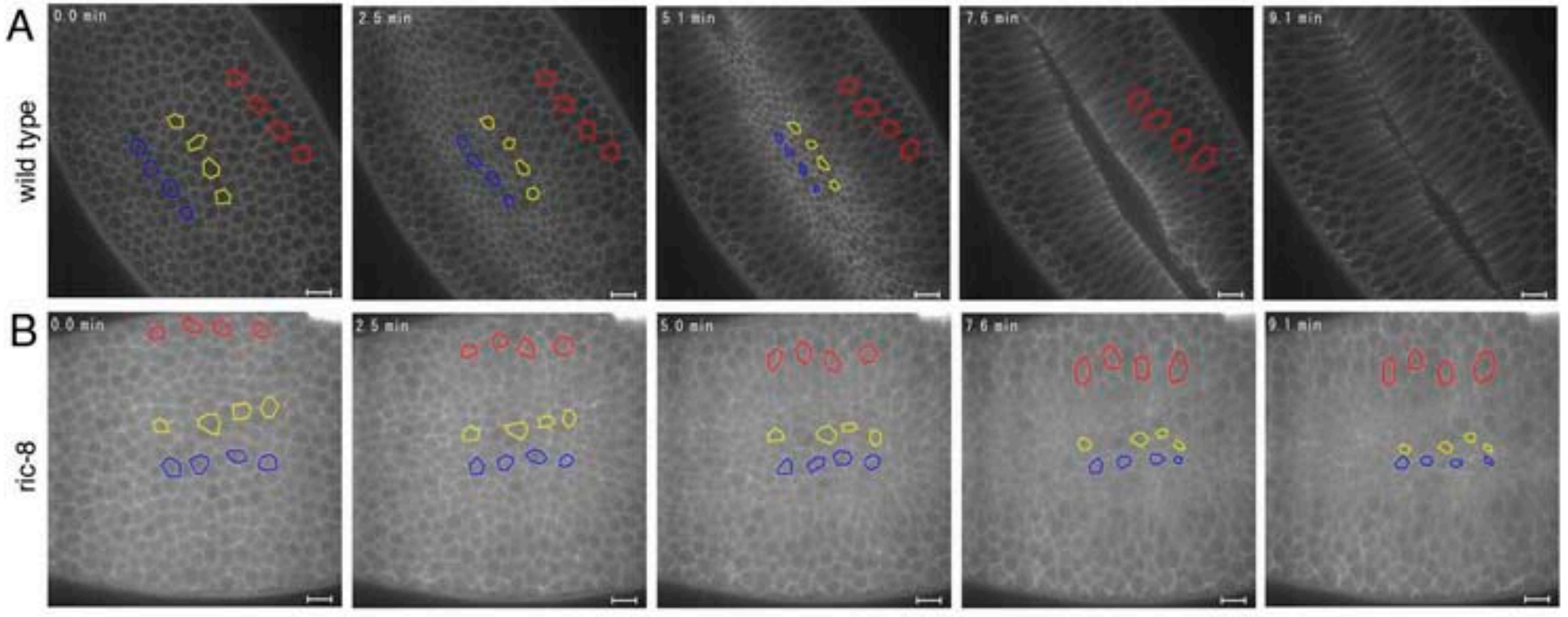
A
wild type
0.0 min
2.5 min
5.1 min
7.6 min
9.1 min
B
ric-8
0.0 min
2.5 min
5.0 min
7.6 min
9.1 min

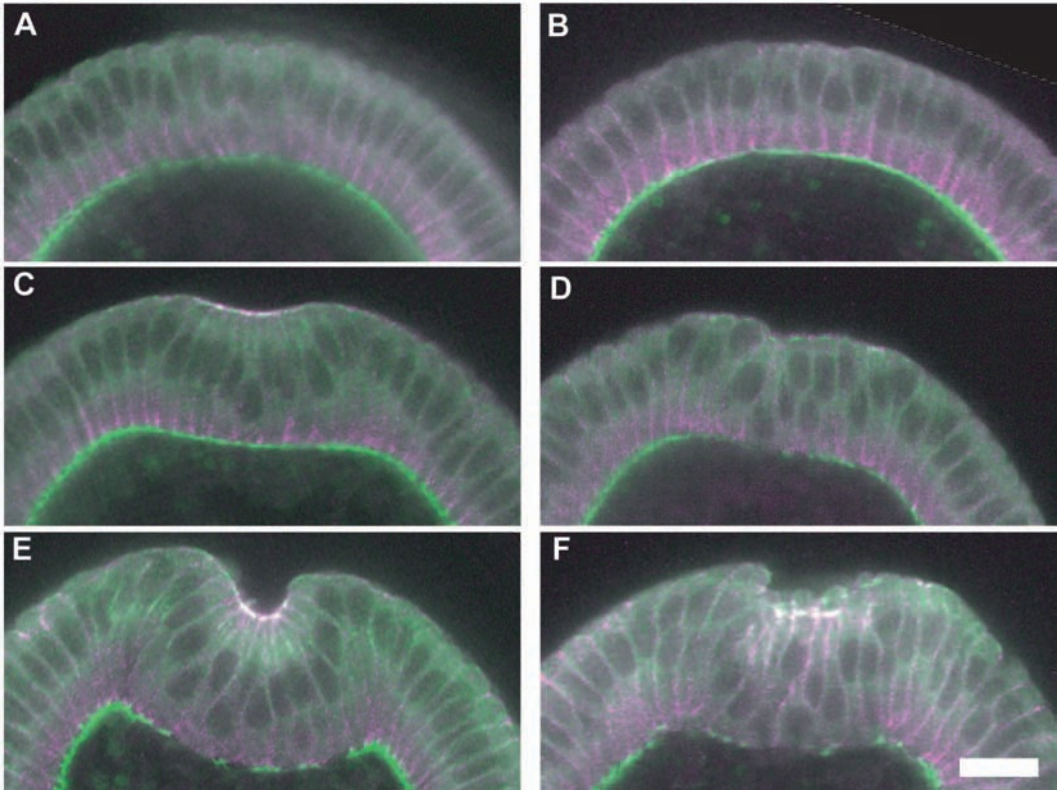
wild type
ric-8
A
B
C
D
E
F

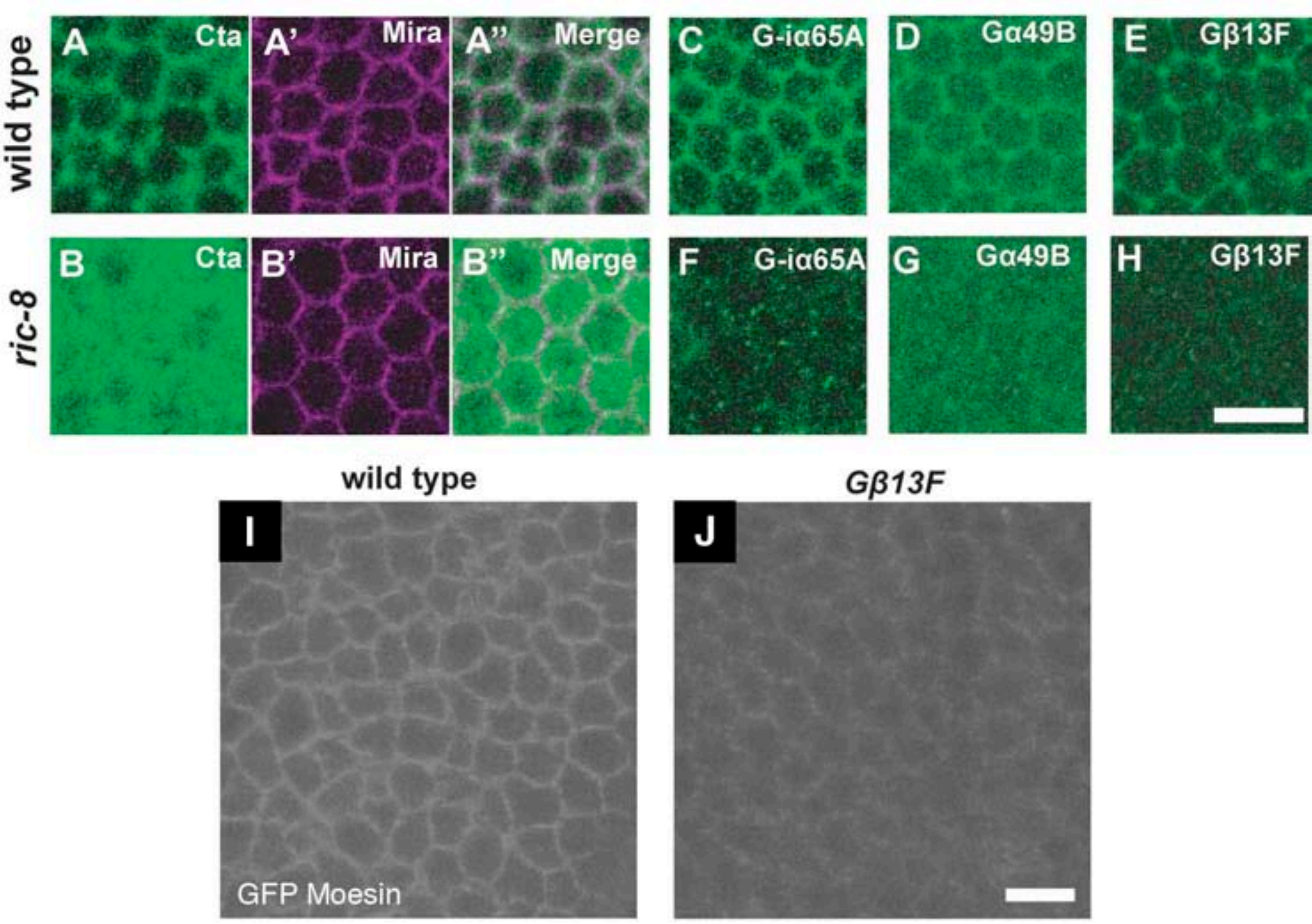
wild type
ric-8
A
Cta
A'
Mira
A''
Merge
C
G-iα65A
D
Gα49B
E
Gβ13F
B
Cta
B'
Mira
B''
Merge
F
G-iα65A
G
Gα49B
H
Gβ13F
wild type
Gβ13F
I
J
GFP Moesin

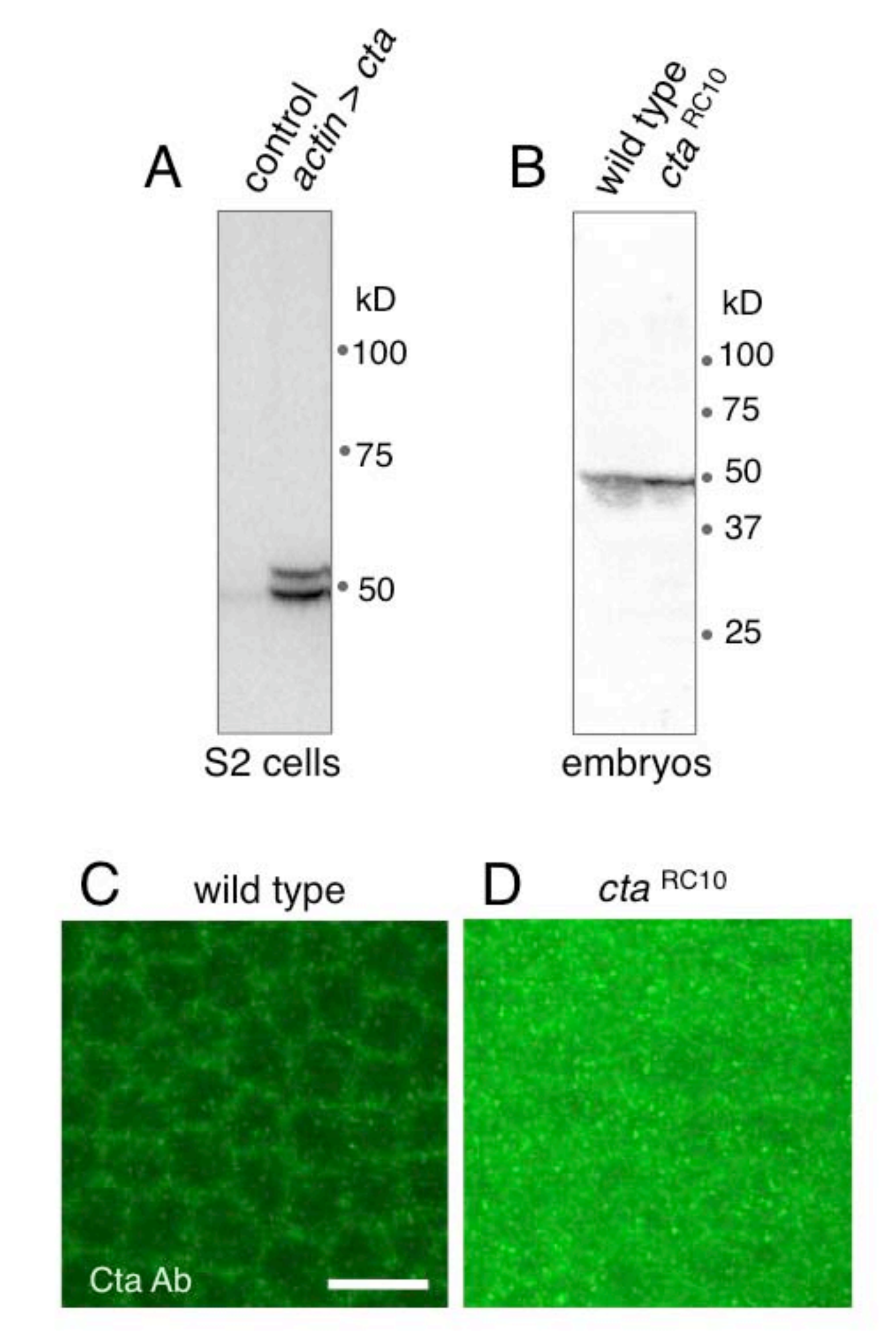
A
control
actin > cta
kD
100
75
50
S2 cells
B
wild type
cta RC10
kD
100
75
50
37
25
embryos
C
wild type
Cta Ab
D
cta RC10